Structure, Optical Properties and Magnetocaloric Effects in Gd₃Fe₅O₁₂ Garnet Synthesized by Solid State Method

C.P. Reshmi[*],[iD] and A.R. Ramesh[*],[iD]

Department of Chemistry, Government Victoria College, Research Center under University of Calicut, Palakkad-678001, India

*Corresponding authors: E-mail: cpreshmi@gvc.ac.in; aroramesh@gvc.ac.in

In this work, gadolinium iron garnet ($Gd_3Fe_5O_{12}$) was synthesized using the solid-state ceramic method. The structural analysis, confirmed through Rietveld refinement, indicated the formation of a single-phase garnet structure. Scanning electron microscopy studies revealed uniform grain size and homogeneity in the sintered material, while UV-vis absorption studies showed a peak at 300 nm, indicating strong ultraviolet interaction and an optical band gap of 3.64 eV, suggesting optoelectronic potential. The fluorescence emission spectrum shows a band at 435 nm, while the excitation spectrum exhibits bands at 275 and 360 nm. The magnetic measurements demonstrated Gd ion ordering at low temperatures, with a compensation temperature around 290 K. Arrott plots confirmed the second-order magnetic phase transition. Importantly, $Gd_3Fe_5O_{12}$ exhibited both normal and inverse magnetocaloric effects, with a maximum magnetic entropy change of 1.05 J kg^{-1} K^{-1} at 230 K under 9 T magnetic field. These properties indicate $Gd_3Fe_5O_{12}$ material as a promising candidate for magnetic refrigeration and optoelectronic applications.

Keywords: Gadolinium iron garnet, Magnetocaloric effect, Compensation temperature, Rietveld refinement, Arrott plot.

INTRODUCTION

The pursuit of advanced materials with multifunctional properties has intensified in recent years, driven by the increasing demand for efficient energy conversion, storage and magnetic refrigeration technologies [1,2]. Among the various classes of materials, garnet-type compounds, especially those based on rare-earth elements (RE garnets), have garnered significant attention due to their distinctive combination of structural, optical and magnetic properties. These materials, represented by the chemical formula $A_3B_2C_3O_{12}$ (where A is a RE^{3+} ion and B and C may be Ga^{3+}, Al^{3+} or Fe^{3+} ions), exhibit unique magnetic and optical characteristics [3,4]. Gadolinium iron garnet ($Gd_3Fe_5O_{12}$ or GdIG) stands out for its exceptional magneto-optical and magneto-dielectric properties, making it a highly promising candidate for various technological applications [5-8].

The dodecahedral (c), octahedral (a) and tetrahedral (d) sites within the garnet structure contribute significantly to their physical properties. These sites accommodate a variety of cations, with 24 A ions, 16 B ions and 24 C ions in the (c), (a) and (d) Wyckoff positions, respectively. Each unit cell of garnet

structure houses 8 formula units, forming a network of metal-oxygen polyhedra. These polyhedra are interconnected, with each tetrahedron linked to four octahedra and each octahedron connects with six tetrahedra, creating a 3D framework. This structural arrangement results in slightly distorted cubic voids that accommodate rare earth ions, leading to the garnet's characteristic space group [9-11].

The magnetic properties of rare earth garnets arise from the antiferromagnetic exchange interactions among the ions at the (a), (d) and (c) sites. GdIG, a ferrimagnetic material, exhibits remarkable magnetic properties driven by interactions between Gd^{3+} and Fe^{3+} ions. In GdIG, the Fe^{3+} ions at the octahedral (a) and tetrahedral (d) sites align antiparallel, resulting in a net magnetic moment, while the Gd^{3+} ions in the dodecahedral (c) sites contribute a weaker magnetic moment. GdIG is characterized by a magnetic compensation temperature, where the net magnetization becomes zero due to the cancellation of the Gd^{3+} and Fe^{3+} sublattice moments [12-14]. Below this temperature, the Gd^{3+} sublattice dominates, while above it, the Fe^{3+} sublattice prevails. GdIG also exhibits a Curie temperature of around 560 K, above which it transition to a paramagnetic state. Its strong

magneto-optical effects, such as Faraday rotation, make it valuable in optical isolators and photonic devices. The magnetic behaviour is further influenced by the antiferromagnetic exchange interactions between the Fe^{3+} ions at the (a) and (d) sites, as well as the interactions between Gd^{3+} and Fe^{3+} ions across different sites. These unique properties position GdIG as an important material for various technological applications, particularly in microwave and magneto-optical devices [5,15-18].

The extensive study on GdIG underscores its importance as a material with significant magnetic and optical properties. Studies continue to explore ways to optimize these properties for a variety of applications, including magnetic sensors, memory devices, optical isolators and advanced photonic systems [19]. Recent developments have highlighted the requirement for a comprehensive understanding of the structure-property relationships in GdIG, particularly in optimizing its magnetocaloric effects for practical applications. While some studies have explored the influence of doping on GdIG's magnetic properties [20,21]. There remains a significant gap in the literature regarding the systematic study of the material's structural and optical characteristics in correlation with its magnetocaloric behaviour. This research aims to address these gaps by providing a detailed analysis of the synthesis, structure and multifunctional properties of GdIG. Using the solid-state approach, this research aims to prove a relationship between the synthesis parameters and the normal and inverse magnetocaloric effects, which would help in developing better materials for magnetic refrigeration and other applications. In this context, the present study investigates the structural, optical, magnetic and magnetocaloric properties of GdIG synthesized *via* the solid-state route. Understanding the magnetic behaviour, including the Curie temperature and magnetic moment, is crucial for evaluating its potential as a magnetic refrigerant. Moreover, exploring both normal and inverse magnetocaloric effects provides insights into the underlying mechanisms and broadens the scope of potential applications.

EXPERIMENTAL

Synthesis of gadolinium iron garnet (GdIG): The synthesis of $Gd_3Fe_5O_{12}$ garnet (GdIG) was achieved using the conventional solid-state ceramic route, a widely used method for producing polycrystalline ceramics [22,23]. In this process, high-purity gadolinium oxide (Gd_2O_3) and iron oxide (Fe_2O_3) powders were used as starting materials. The respective oxides of Gd and Fe were weighed and mixed in the stoichiometric proportions to achieve the desired chemical composition of GdIG. The mixed powder was then subjected to ball milling using distilled water to form a homogeneous slurry. The homogeneous mixture was then dried and subjected to calcination at 1300 ℃ for 12 h, to promote solid-state reactions between the components, leading to the formation of garnet phase. After calcination, the sample was ground, pressed and sintered at 1400 ℃ for 2 h, to strengthen the material and enhance its crystalline quality.

Characterization: The X-ray diffraction (XRD) pattern of GdIG was recorded using a PANalytical X'Pert Pro diffractometer with copper *K*α radiation. The scan covered a 2θ range

from 10º to 90º, with a step size of 0.017º and a scan step time of 40.702 s per step. Microstructure studies of the sintered sample were done by scanning electron microscope (SEM, Hitachi S3400).The magnetization measurements were conducted with varying temperature and applied magnetic field using a vibrating sample magnetometer (VSM). The resulting magnetization data were used to calculate the change in magnetic entropy $(-\Delta S_M)$ by applying the Maxwell's equation [24]:

$$\Delta S_m(T, \Delta H) = \int_{H_1}^{H_2} \left(\frac{\delta M(T,H)}{\delta T} \right)_H dH \qquad (1)$$

The magnetization isotherms measured at 5 K intervals were used in the computations.

The ultraviolet-visible (UV-vis) absorption spectrum of the GdIG was obtained using a Shimadzu UV-3600 double-beam spectrophotometer. The emission spectrum was recorded using a Jobin Yvon SPEX-Fluorolog 3 (Horiba) spectrofluorometer, with a 450 W xenon arc lamp serving as the excitation light source. Both excitation and emission monochromators were employed and emitted photons were detected using a photomultiplier tube detector.

RESULTS AND DISCUSSION

Structural studies: The X-ray diffraction data of GdIG was collected and subjected to Rietveld refinement with GSAS software to obtain the lattice parameters, unit cell volume, space group and atomic positions (Table-1) [25]. The initial parameters

TABLE-1
STRUCTURAL PARAMETERS OF
Gd₃Fe₅O₁₂ AFTER RIETVELD REFINEMENT

Material	GdIG
Space group	$Ia\bar{3}d$
Lattice parameter, a (Å)	12.47135 (7)
Volume (Å³)	1939.72 (3)
Atomic positions	
Gd(c) x	0.125
Gd(c) y	0
Gd(c) z	0.25
Fe(a) x	0
Fe(a) y	0
Fe(a) z	0
Fe(d) x	0.375
Fe(d) y	0
Fe(d) z	0.25
O x	-0.0347
O y	0.0549
O z	0.1503
Bond angle (°)	
$Fe^{3+}_{(a)} - O - Fe^{3+}_{(d)}$	129.408
$Gd^{3+}_{(c)} - O - Gd^{3+}_{(c)}$	101.324
$Fe^{3+}_{(a)} - O - Gd^{3+}_{(c)}$	100.020, 101.530
$Fe^{3+}_{(d)} - O - Gd^{3+}_{(c)}$	92.971, 124.358
Bond length (Å)	
$Fe^{3+}_{(a)} - O^{2-}_{(h)}$	2.04 (6)
$Fe^{3+}_{(d)} - O^{2-}_{(h)}$	1.81 (4)
$Gd^{3+}_{(c)} - O^{2-}_{(h)}$	2.44 (4), 2.49 (4)
Goodness of fit	
Rwp %	6.51
Rp %	5.13

for the Rietveld refinement of GdIG were obtained from the known structural data of $Gd_3Fe_5O_{12}$ single crystal [26]. The monophasic garnet structure of GdIG was ascertained by the Rietveld analysis and was found to crystallize in the cubic space group, $Ia\bar{3}d$. The most prominent reflection peaks observed in the XRD pattern (Fig. 1a) correspond to the (211), (420), (321), (400), (422), (521) and (611) planes, which are characteristic of the garnet lattice and indicative of garnet-type materials. The refined XRD patterns of GdIG are also consistent with the expected garnet structure, validating the refinement process. The refined structural parameters, including lattice constants and atomic positions, were determined with high precision. Additionally, the $Fe^{3+}_{(a)} - O^{2-}_{(h)}$, $Fe^{3+}_{(d)} - O^{2-}_{(h)}$, $Gd^{3+}_{(c)} - O^{2-}_{(h)}$ bond lengths and $Fe^{3+}_{(a)} - O - Fe^{3+}_{(d)}$, $Gd^{3+}_{(c)} - O - Gd^{3+}_{(c)}$, $Fe^{3+}_{(a)} - O - Gd^{3+}_{(c)}$, $Fe^{3+}_{(d)} - O - Gd^{3+}_{(c)}$ bond angles were also estimated from the refinement and all are consistent with the result obtained in the literature (Table-1) [26].

The SEM study was conducted on sintered pellet of GdIG to investigate their microstructural characteristics and is depicted in Fig. 1b. The SEM analysis revealed that the sintered GdIG pellet exhibits a well-defined grain structure. The grain bounda-ries were observed to be clean and distinct, indicating effective densification during the sintering process. The micrographs showed that the grains are closely packed, suggesting minimal porosity. Additionally, the uniform grain size distribution in the range of 1 to 8 μm across the pellet surface reflects the homogeneous nature of the material.

Optical studies: The UV-vis absorption spectrum (Fig 2a) of $Gd_3Fe_5O_{12}$ garnet exhibits a broad absorption range from 250 to 410 nm, with a pronounced absorption peak at 300 nm, indicating strong interaction with ultraviolet light. The optical band gap was determined to be 3.64 eV, as calculated from the Tauc plot (Fig. 2b), which suggests the material has potential applications in optoelectronic devices. The fluorescence emis-sion spectrum spans from 350 to 625 nm, with a significant emission peak at 435 nm (Fig. 3a). Additionally, the excitation spectra revealed two distinct bands with maxima at 275 and 360 nm, corresponding to the energy levels involved in the optical transitions (Fig. 3b).

Magnetic studies: The M-T curve of GdIG offers valuable insights into the magnetic behaviour of the material across various temperature ranges. Both zero field cooled (ZFC) and
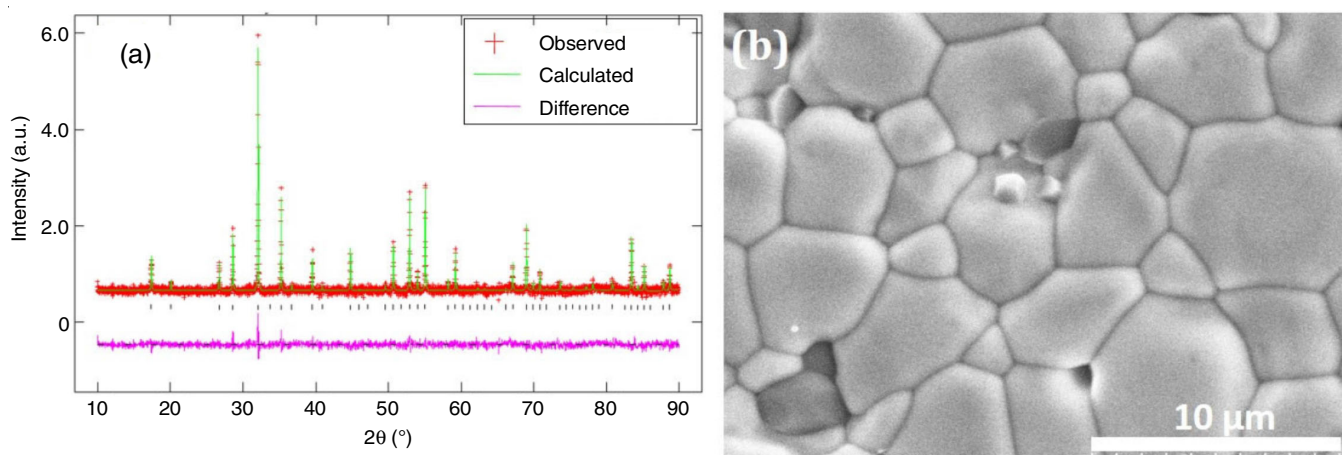

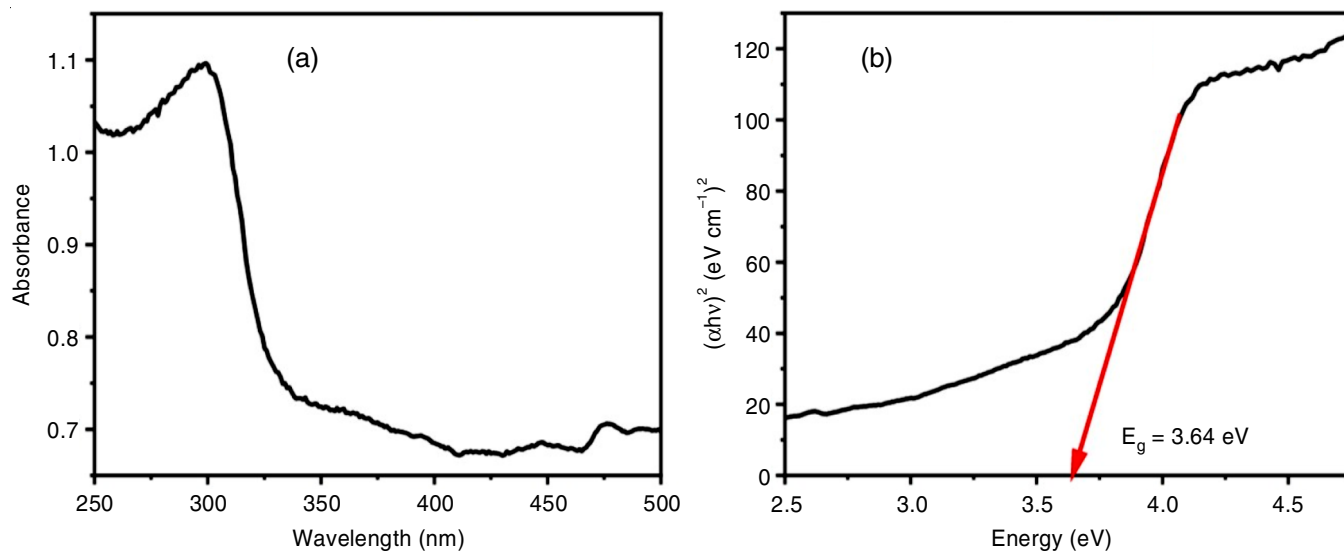Fig. 1. (a) Rietveld refined XRD pattern and (b) SEM image of GdIG

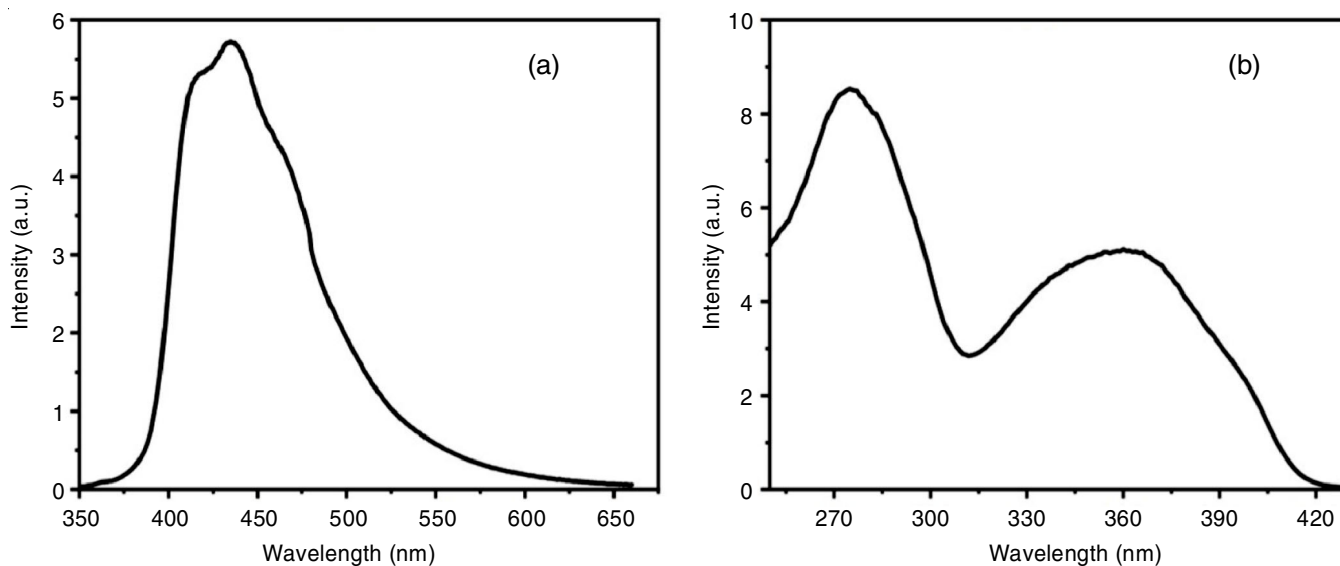Fig. 2. (a) UV-vis absorption spectrum and (b) Tauc plot of GdIG

Fig. 3. (a) Emission spectrum and (b) excitation spectrum of GdIG

field cooled (FC) magnetization data were collected at 0.01 T magnetic field (Fig. 4). Previous reports showed that GdIG exhibits paramagnetic behaviour at high temperature and a transition to ferrimagnetic state as the temperature decreases, with a Curie temperature (T_C) of ~ 560 K [27,28]. In the present study, the temperature dependence of magnetization was examined from 2 K to 380 K to investigate the precise magnetic behaviour of GdIG. The M-T curve shows high magnetization at lower temperatures due to the ordering of the Gd^{3+} sublattice [29,30], followed by a gradual decrease as the temperature rises to about 200 K. Beyond this point, the magnetization decreases more rapidly, reaching zero around 290 K in the ZFC curve. This sharp decline corresponds to the compensation point (T_{COMP}), a distinctive feature of rare earth iron garnets, where the magnetic moments of Gd^{3+} and Fe^{3+} sublattices cancel each other out, leading to net zero magnetization [31,32]. After the compensation temperature, the magnetization increases again as the Fe^{3+} ions in the octahedral and tetrahedral sublattices align antiparallel to each other due to strong ferrimagnetic coupling
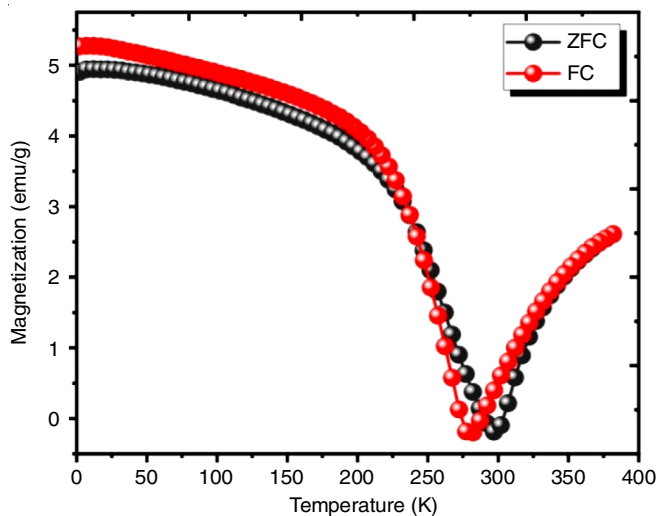

Fig. 4. M-T curve of GdIG (at 0.01 T)

[31]. The M-T curve of GdIG thus reflects the intricate interplay of ferrimagnetic interactions within the material, highlighted by the compensation point and the alignment of the Gd^{3+} ions at low temperatures [32].

Based on the M-T data, the magnetocaloric effect in GdIG is particularly interesting due to the compensation effect and significant magnetization observed at low temperatures. The magnetic field dependence of magnetization was recorded across two temperature ranges: 225 K to 290 K (Fig. 5a) and 295 K to 350 K (Fig. 5b). In Fig. 5a, GdIG exhibits strong magnetization, which is attributed to the large magnetic moment of Gd^{3+} ions [33]. The magnetization shows a clear response to the applied magnetic field, with no saturation observed within the measured field range at lower temperatures. Fig. 5b displays the M-H behaviour of GdIG after the compensation point, highlighting the non-saturating nature of the M-H curve. This behaviour is indicative of the ferrimagnetic coupling between Fe^{3+} ions at the (a) and (d) sites [31]. The Arrott plots for GdIG garnet are shown in Fig. 5c-d to further explore its magnetic properties. All the curves exhibit a positive slope, which indicates that GdIG undergoes a second-order magnetic phase transition within the measured temperature range. This suggests that the energy loss due to thermal hysteresis is minimal in GdIG [34].

From the M-H data at different temperatures, the magnetic entropy change ($-\Delta S_M$) for GdIG was calculated using Maxwell's relation (eqn. 1). Fig. 6 shows the temperature dependence of $-\Delta S_M$ under different magnetic fields, where the absolute value of $-\Delta S_M$ increases with the application of a stronger magnetic field. GdIG displays a normal magnetocaloric effect ($-\Delta S_M >$ 0), with the sign of $-\Delta S_M$ reversing at a certain temperature, indicative of the compensation point unique to heavy rare earth iron garnets [32]. For the normal magnetocaloric effect, $-\Delta S_M$ reaches a maximum of 1.05 J kg^{-1} K^{-1} at T = 230 K under a magnetic field of H = 9 T. As the temperature increases $-\Delta S_M$ decreases rapidly, approaching zero as the temperature nears the compensation point. Beyond the compensation temperature, it displays the maximum inverse magnetocaloric effect,
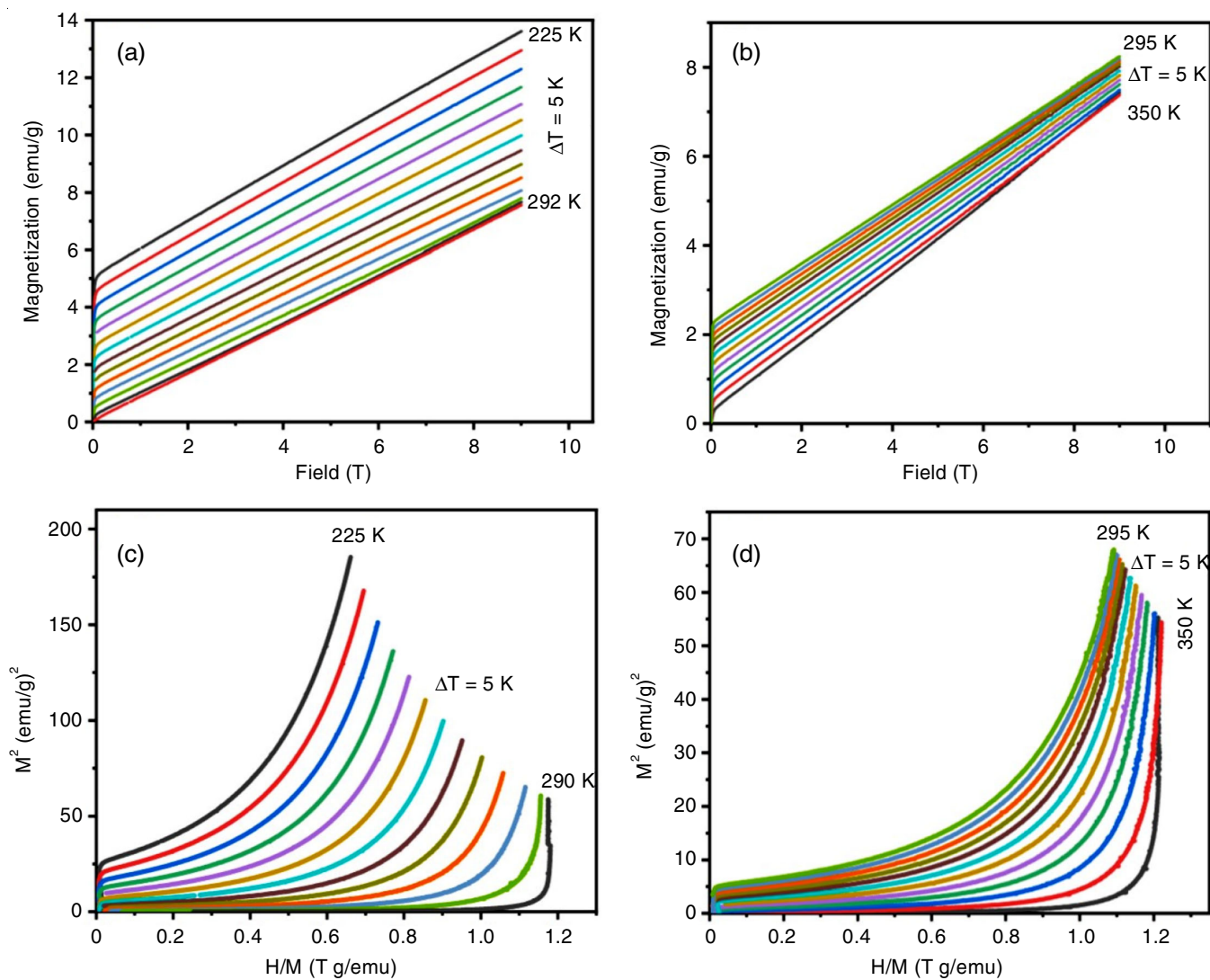
Fig. 5. (a,b) Field dependent magnetization curves of GdIG before and after T_{COMP}; (c,d) Arrott plots of GdIG before and after T_{COMP}
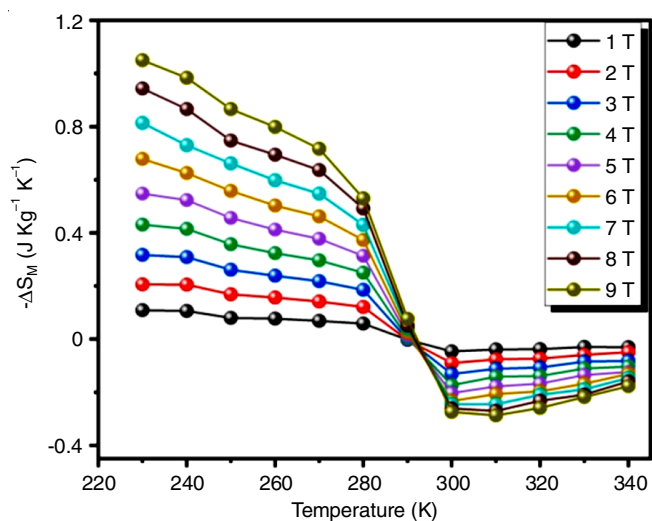

Fig. 6. Temperature dependence of magnetic entropy change of GdIG

then again trends toward zero. This behaviour underscores the potential of GdIG in magnetic refrigeration applications, particularly within the temperature ranges where the magnetocaloric

effect is most pronounced. The observation of both normal and inverse magnetocaloric effects in GdIG is linked to the complex magnetic interactions within the material, especially involving gadolinium ions and the iron sublattice.

The field-dependent magnetic entropy change ($-\Delta S_M$) in a material is a measure of the change in entropy under the influence of magnetic field, typically observed during a magnetic phase transition [35,36]. In magnetic systems like GdIG, the application of a magnetic field causes the magnetic moments to align, leading to a reduction in magnetic entropy and the release or absorption of heat, depending on the nature of the magnetocaloric effect. The magnitude of ΔS_M is influenced by the strength of the applied field and the specific temperature at which the phase transition occurs, with maximum changes often observed near critical temperatures such as the Curie temperature or spin reorientation temperature [35,37]. A linear relationship between $\ln(-\Delta S_M)$ and $\ln(H)$ was analyzed from 230 K to 280 K (Fig. 7a) and at the compensation point (Fig. 7b). The slope of these plots yielded the value of n, which was then plotted against temperature from 230 K to 280 K (Fig. 8). The constant value of n across this temperature range suggests
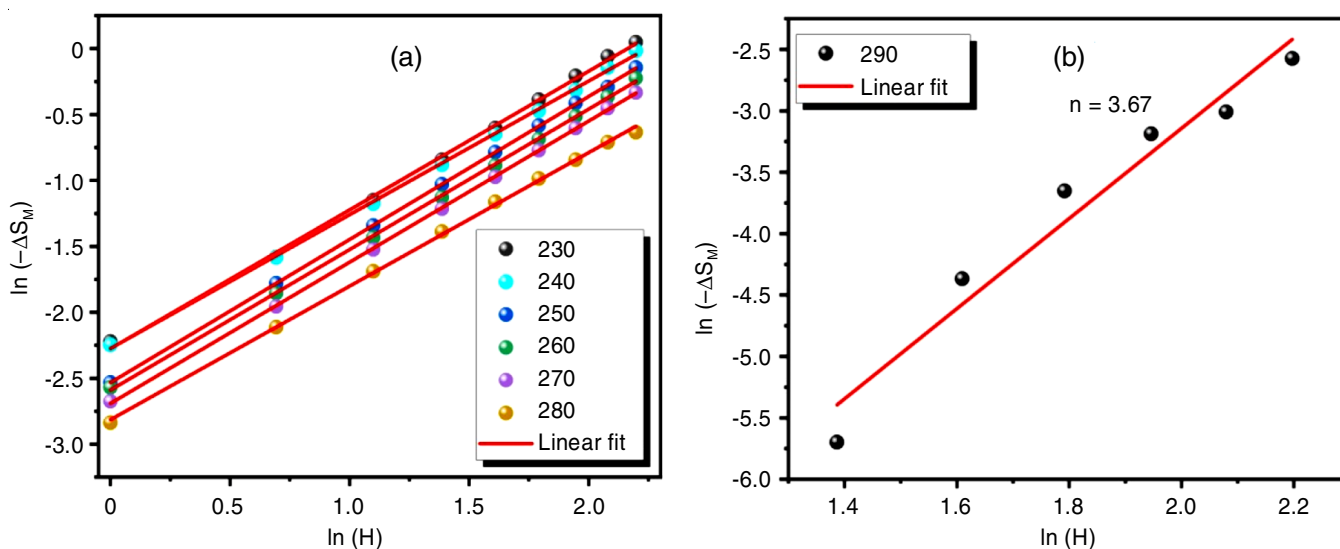
Fig. 7. (a) Linear plot of ln(-ΔS_M) *vs.* ln(H) from 230 to 280 K and (b) at 290 K of GdIG
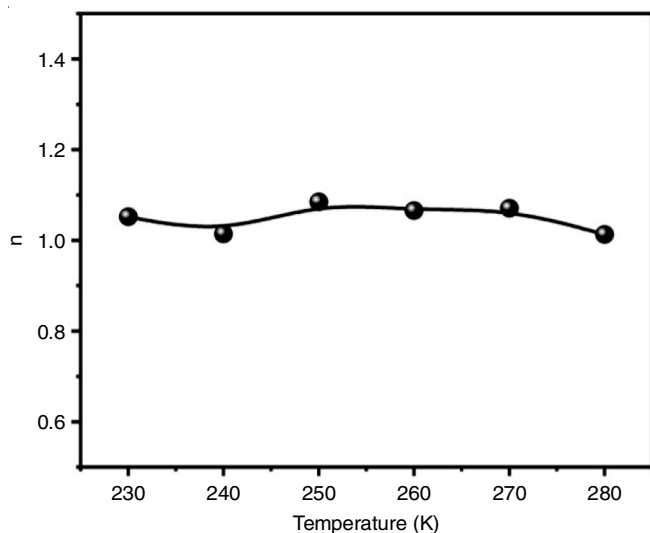

Fig. 8. Temperature dependence of exponent, n of GdIG

similar magnetic interactions within this interval, while the distinct value of *n* at the compensation temperature indicates the presence of different magnetic interactions at that specific temperature.

Conclusion

Gadolinium iron garnet (Gd₃Fe₅O₁₂) was successfully synthesized *via* the solid-state ceramic method, with structural analysis confirming a single-phase garnet structure. The material exhibited uniform grain size and homogeneity, as revealed by SEM. The optical characterization demonstrated strong ultraviolet interaction, with a UV-vis absorption peak at 300 nm and an optical band gap of 3.64 eV, highlighting its potential for optoelectronic applications. Fluorescence and excitation spectra further supported the material's suitability for these applications. Magnetic measurements revealed Gd ion ordering at low temperatures and identified a compensation temperature around 290 K. The second-order nature of the magnetic phase transition was confirmed by Arrott plots. Remarkably, Gd₃Fe₅O₁₂

displayed both normal and inverse magnetocaloric effects, with a maximum magnetic entropy change of 1.05 J kg⁻¹ K⁻¹ at 230 K under a 9 T magnetic field. These results emphasize Gd₃Fe₅O₁₂ as a promising candidate for both magnetic refrigeration and optoelectronic applications, making it a versatile material for advanced technological applications.

CONFLICT OF INTEREST

The authors declare that there is no conflict of interests regarding the publication of this article.

REFERENCES

1. M.I.A.A. Maksoud, R.A. Fahim, A.E. Shalan, M.A. Elkodous, S.O. Olojede, A.I. Osman, C. Farrell, A.H. Al-Muhtaseb, A.S. Awed, A.H. Ashour and D.W. Rooney, *Environ. Chem. Lett.*, **19**, 375 (2021); https://doi.org/10.1007/s10311-020-01075-w
2. B. Monfared and B. Palm, *Int. J. Refrig.*, **96**, 25 (2018); https://doi.org/10.1016/j.ijrefrig.2018.08.012
3. V.I. Nizhankovskiy, *J. Alloys Compd.*, **852**, 156938 (2021); https://doi.org/10.1016/J.JALLCOM.2020.156938
4. Z.T. Karipbayev, K. Kumarbekov, I. Manika, A. Dauletbekova, A.L. Kozlovskiy, D. Sugak, S.B. Ubizskii, A. Akilbekov, Y. Suchikova and A.I. Popov, *Phys. Status Solidi., C Curr. Top. Solid State Phys.*, **259**, 2100415 (2022); https://doi.org/10.1002/pssb.202100415
5. S.I. El Dek and R.M. Amin, *Radiat. Phys. Chem.*, **204**, 110709 (2023); https://doi.org/10.1016/j.radphyschem.2022.110709
6. P.B.A. Fechine, R.S.T. Moretzsohn, R.C.S. Costa, J. Derov, J.W. Stewart, A.J. Drehman, C. Junqueira and A.S.B. Sombra, *Microw. Opt. Technol. Lett.*, **50**, 2852 (2008); https://doi.org/10.1002/mop.23824
7. S. Verma and S. Ravi, *J. Mater. Sci. Mater. Electron.*, **34**, 1011 (2023); https://doi.org/10.1007/s10854-023-10451-5
8. C. Holzmann, A. Ullrich, O.-T. Ciubotariu and M. Albrecht, *ACS Appl. Nano Mater.*, **5**, 1023 (2022); https://doi.org/10.1021/acsanm.1c03687

9. F. Maglia, V. Buscaglia, S. Gennari, P. Ghigna, M. Dapiaggi, A. Speghini and M. Bettinelli, *J. Phys. Chem. B*, **110**, 6561 (2006); https://doi.org/10.1021/jp055713o

10. R. Krsmanovic, V.A. Morozov, O.I. Lebedev, S. Polizzi, A. Speghini, M. Bettinelli and G.V. Tendeloo, *Nanotechnology*, **18**, 325604 (2007); https://doi.org/10.1088/0957-4484/18/32/325604

11. C.A. Cortés-Escobedo, A.M. Bolarín-Miró, F.S.-D. Jesús, R. Valenzuela, E.P. Juárez-Camacho, I.L. Samperio-Gómez and S. Ammar, *Adv. Mater. Phys. Chem.*, **03**, 41 (2013); https://doi.org/10.4236/ampc.2013.31A006

12. D. Rodic, Z. Tomkowicz, L. Novakovic, A. Szytula and M.L. Napijalo, *Solid State Commun.*, **73**, 243 (1990); https://doi.org/10.1016/0038-1098(90)90966-F

13. Sh.M. Aliev, I.K. Kamilov, M.Sh. Aliev and Zh.G. Ibaev, *Phys. Solid State*, **56**, 1114 (2014); https://doi.org/10.1134/S106378341406002X

14. A.B. Cahaya, A. Azhar, D. Djuhana and M.A. Majidi, *Phys. Lett. A*, **437**, 128085 (2022); https://doi.org/10.1016/j.physleta.2022.128085

15. Y.R. Uhm, J.C. Lim, S.M. Choi and C.S. Kim, *J. Magn.*, **21**, 303 (2016); https://doi.org/10.4283/JMAG.2016.21.3.303

16. P.B.A. Fechine, H.H.B. Rocha, R.S.T. Moretzsohn, J.C. Denardin, R. Lavín and A.S.B. Sombra, *IET Microw. Antennas Propag.*, **3**, 1191 (2009); https://doi.org/10.1049/iet-map.2008.0301

17. A. Sharma, S.K. Godara and A.K. Srivastava, *Indian J. Phys. Proc. Indian Assoc. Cultiv. Sci.*, **96**, 4173 (2022); https://doi.org/10.1007/s12648-022-02365-5

18. F.N. Shafiee, R.S. Azis, I. Ismail, R. Nazlan, I.R. Ibrahim and A.S.A. Rahim, *Diffus. Defect Data Solid State Data Pt. B Solid State Phenom.*, **268**, 287 (2017); https://doi.org/10.4028/www.scientific.net/SSP.268.287

19. P. Hansen, K. Witter and W. Tolksdorf, *Phys. Rev. B Condens. Matter*, **27**, 4375 (1983); https://doi.org/10.1103/PhysRevB.27.4375

20. Q.I. Mohaidat, M. Lataifeh, S.H. Mahmood, I. Bsoul and M. Awawdeh, *J. Supercond. Nov. Magn.*, **30**, 2135 (2017); https://doi.org/10.1007/s10948-017-4003-y

21. D.T.T. Nguyet, N.P. Duong, T. Satoh, L.N. Anh and T.D. Hien, *J. Magn. Magn. Mater.*, **332**, 180 (2013); https://doi.org/10.1016/j.jmmm.2012.12.031

22. M. Pianassola, M. Loveday, J.W. McMurray, M. Koschan, C.L. Melcher and M. Zhuravleva, *J. Am. Ceram. Soc.*, **103**, 2908 (2020); https://doi.org/10.1111/jace.16971

23. Y.-P. Fu, C.-C. Chang, C.-H. Lin and T.-S. Chin, *Ceram. Int.*, **30**, 41 (2004); https://doi.org/10.1016/S0272-8842(03)00059-2

24. R.D. McMichael, J.J. Ritter and R.D. Shull, *J. Appl. Phys.*, **73**, 6946 (1993); https://doi.org/10.1063/1.352443

25. A.C. Larson and R.B. Von Dreele, General Structure Analysis System (GSAS), Los Alamos National Laboratory Report LAUR, pp. 86-748 (2004).

26. J.E. Weidenborner, *Acta Crystallogr.*, **14**, 1051 (1961); https://doi.org/10.1107/S0365110X6100303X

27. C.N. Chinnasamy, J.M. Greneche, M. Guillot, B. Latha, T. Sakai, C. Vittoria and V.G. Harris, *J. Appl. Phys.*, **107**, 09A512 (2010); https://doi.org/10.1063/1.3357326

28. R. Pauthenet, *J. Appl. Phys.*, **29**, 253 (1958); https://doi.org/10.1063/1.1723094

29. C. Cascales, M.T. Fernández Díaz and M.A. Monge, *Chem. Mater.*, **12**, 3369 (2000); https://doi.org/10.1021/cm0011209

30. J. Jensen and A.R. Mackintosh, Rare Earth Magnetism, Structures and Excitations, Clarendon Press: Oxford (1991).

31. J. Sultana, J. Mohapatra, J.P. Liu and S.R. Mishra, *AIP Adv.*, **13**, 025252 (2023); https://doi.org/10.1063/9.0000519

32. C. Li, Y. Qiu, G.O. Barasa and S. Yuan, *Ceram. Int.*, **46**, 18758 (2020); https://doi.org/10.1016/j.ceramint.2020.04.191

33. Aakansha, and S. Ravi, *Mater. Res. Express*, **6**, 126113 (2020); https://doi.org/10.1088/2053-1591/ab62e7

34. W. Dunhui, T. Shaolong, H. Songling, Z. Jianrong and D. Youwei, *J. Magn. Magn. Mater.*, **268**, 70 (2004); https://doi.org/10.1016/S0304-8853(03)00474-8

35. V. Franco, J.S. Blázquez and A. Conde, *Appl. Phys. Lett.*, **89**, 222512 (2006); https://doi.org/10.1063/1.2399361

36. Q.Y. Dong, H.W. Zhang, J.R. Sun, B.G. Shen and V. Franco, *J. Appl. Phys.*, **103**, 116101 (2008); https://doi.org/10.1063/1.2913166

37. V. Franco, A. Conde, J.M. Romero-Enrique, Y.I. Spichkin, V.I. Zverev and A.M. Tishin, *J. Appl. Phys.*, **106**, 103911 (2009); https://doi.org/10.1063/1.3261843